High-fidelity entanglement of polar molecules by dynamic geometric control

Scarlett S. Yu,[1,2] Avikar Periwal,[1,2,3] Jiaqi You,[1,2] Zirui Liu,[4] Qinshu Lyu,[5] Youngju Cho,[6] Loïc Anderegg,[7] Eunmi Chae,[6] and John M. Doyle[1,2]

[1]*Department of Physics, Harvard University, Cambridge, MA 02138, USA*
[2]*Harvard-MIT Center for Ultracold Atoms, Cambridge, MA 02138, USA*
[3]*Department of Physics, Massachusetts Institute of Technology, Cambridge, MA 02139, USA*
[4]*Institute for Interdisciplinary Information Sciences, Tsinghua University, Beijing 100084, PR China*
[5]*Centre for Cold Matter, Blackett Laboratory, Imperial College London, London SW7 2AZ, United Kingdom*
[6]*Department of Physics, Korea University, Seongbuk-gu, Seoul 02841, South Korea*
[7]*Department of Physics and Astronomy, University of Southern California, Los Angeles, CA 90089, USA*

In quantum information systems made of optical tweezer arrays of ultracold molecules, thermal motion of molecules degrades the coherence of their interactions, which limits entanglement fidelity and the concomitant scientific applicability of these systems. We show that by controlling the geometry of the dipolar interaction, even when a molecule occupies many motional states in the tweezer, coherence can be preserved. We characterize several geometries that suppress sensitivity to thermal fluctuations. We further use programmable, coherence-preserving motion of the molecules during entanglement to refocus dephasing from relative positional jitter of the tweezers, which is relevant even on the 10 nm scale. These methods yield substantially improved dipolar coherence and enable generation of two-molecule entanglement with a Bell state fidelity of $\mathcal{F} = 0.976^{+0.008}_{-0.011}$ in directly laser-cooled molecules.

INTRODUCTION

A defining requirement for quantum simulation and quantum information processing is the ability to generate entanglement through controlled interactions. Polar molecules offer a compelling combination of quantum resources, including long-lived rotational transitions [1–5], rich internal state manifolds for multilevel encoding [5–7], and molecular electric dipole moments that enable long-range entangling interactions [8–11]. Notably, rotational qubits can be easily tuned and controlled using microwave and dc electric fields [12–15]. The capabilities of these qubits suggest new routes to quantum simulation of many-body spin dynamics [15–23], quantum information processing [6, 24–28], and precision laboratory searches for both dark matter [29, 30] and new CP-violating particles in the $> 10\,\mathrm{TeV}$ range [31–34]. Recent experiments have realized dipolar spin exchange interactions and Bell state creation between individual molecules in optical tweezers [8–11, 21], placing molecular systems in a practical regime for quantum simulation of interacting spin models and entangling operations for digital quantum information processing.

The coherent quantum dynamics of two interacting molecules is driven by the dipolar coupling (J), with strength that depends on the relative displacement vector $\vec{r}$ between the molecules and their orientation with respect to the quantization field axis. Changes in $\vec{r}$ translate into changes in the entanglement rate. A central limitation for coherent dipolar driven entanglement is dephasing induced by thermal motion of molecules. Thermal occupation of many motional states leads to a distribution of effective interaction strengths. For molecules trapped in optical tweezers, the weak confinement along the longer tweezer beam axis makes the molecular positional wave packet strongly anisotropic, and is the dominant contribution to dephasing for previous demonstrations of entanglement in polar molecules [10, 11]. The few quanta of motional excitation provided a fundamental limit on interaction coherence. This motivates finding new strategies to suppress sensitivity of J to thermal fluctuations by narrowing the distribution of effective coupling strengths sampled across experimental realizations to improve many-body coherence [27, 35, 36]. In this work, we utilize both static and dynamic geometrical programming to control and improve coherence in two-qubit entanglement of molecules in an optical tweezer array. We first experimentally demonstrate that static geometry engineering can suppress thermal dephasing by realizing interaction configurations that minimize sensitivity to motional fluctuations. Under optimal conditions, trap position fluctuations on the order of a few nanometers become the dominant source of dephasing. We take advantage of the long rotational coherence time of molecules to implement a geometric echo protocol that changes the relative molecular positions during dipolar entangling, effectively refocusing positional noise. This demonstration of coherent molecular locomotion highlights that programmable trap motion can be used not only for assembly and rearrangement, but as a coherent rectifying operation during interactions. With the addition of partial Raman sideband cooling, higher-order thermal effects are suppressed to realize a two-molecule Bell state with a measured fidelity of $\mathcal{F} = 0.976^{+0.008}_{-0.011}$. This result, to our knowledge, is the highest reported fidelity for directly laser-cooled molecules, and is comparable to state-of-the-art demonstrations of entanglement between assembled molecules [10, 11]. The power of these

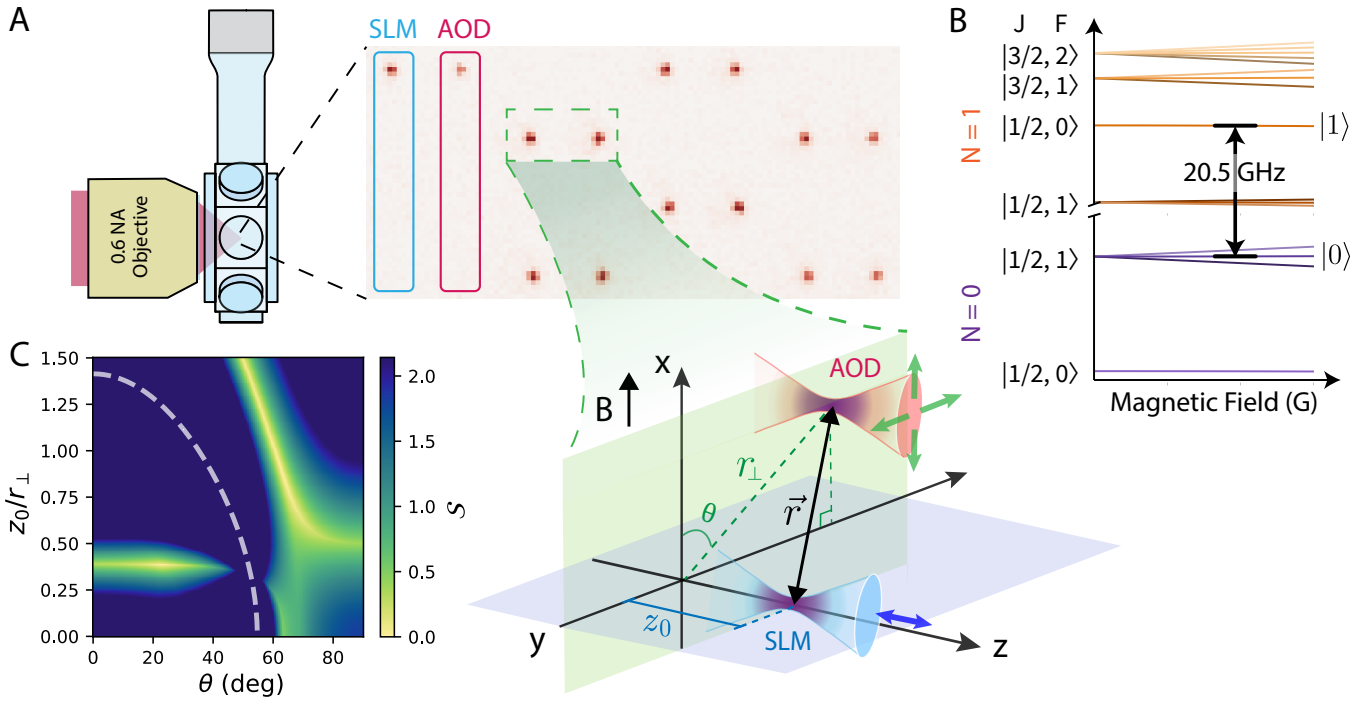

FIG. 1. **Three-dimensional geometric control of dipolar interactions in a molecular tweezer array.** (**A**) Schematic of the optical tweezer array and geometric coordinates used in this work. CaF (calcium monofluoride) molecules are loaded into 775 nm optical tweezers projected through a 0.6 NA microscope objective into a vacuum glass cell. Inset: Geometry and coordinates between one pair of interacting molecules. The tweezer propagation is along $\hat{z}$. The relative separation vector between two molecules is $\vec{r} = \vec{r}_\perp + z_0\hat{z}$, where $\vec{r}_\perp$ is the in-plane separation and z_0 is their relative axial displacement. The angle θ is defined between $\vec{r}_\perp$ and the quantization axis, which is set by a small applied magnetic field along $\hat{x}$. One trap (shown in red) is generated from crossed 2D-AODs, which provide lateral positioning to set $(r_\perp, \theta)$, while the other trap (shown in blue) is projected from an SLM phase mask, which can independently impose z_0. (**B**) Relevant internal state manifolds used in preparing and defining the rotational qubit. (**C**) Dipolar motional sensitivity in experimentally accessible three-dimensional geometry. Color shows the dimensionless weighted relative sensitivity $\mathcal{S}$, defined in main text, of the interaction strength to thermally-induced dephasing. The dashed curve marks $J = 0$; brighter regimes indicate reduced leading-order sensitivity to thermal motion.

methods is highlighted because the molecular temperatures here are much higher. This sets a firm, realistic path to fidelities well above the 99% level, as first envisioned by theory [27, 35].

Our experiment is carried out with laser-cooled calcium monofluoride (CaF) molecules individually trapped in a two-dimensional (2D) optical tweezer array, illustrated in Fig. 1A. We first describe the tweezer architecture relevant to geometric control of dipolar interactions. (Molecule production, laser cooling, and trapping of CaF have been described in detail in previous work [37, 38]). The tweezer array is formed from two beam paths derived from the same laser: in one path, the light is reflected by a spatial light modulator (SLM), which generates a static array, while the other beam is diffracted by two crossed acousto-optic deflectors (2D-AODs) to create a set of dynamic tweezers. The two beams are combined and projected through the microscope objective. One trap of an interacting pair of molecules is generated by the SLM and the other by the AODs. The SLM defines a static two-dimensional array and the trap position in the axial direction, while the AODs provide rapid motion in the lateral directions. This architecture allows convenient access to the three-dimensional interaction geometry between pairs of directly laser-cooled CaF molecules, and avoids using multi-tone AOD operation which can introduce parametric heating [39].

Molecules are initially loaded and rearranged into a 2D array in the SLM tweezers with 14 μm spacing. We encode a qubit in two rotational states $|\uparrow\rangle \equiv |X; \nu = 0, N = 1, F = 0, m_F = 0\rangle$ and $|\downarrow\rangle \equiv |X; \nu = 0, N = 0, F = 1, m_F = 0\rangle$ within the electronic and vibrational ground state $X^2\Sigma^+$ of CaF (see Fig. 1B). All molecules are initialized in the qubit state $|\uparrow\rangle$. We then transfer half of the molecules from the SLM tweezers into the dynamic AOD tweezers (see Fig. 1A), and move each molecule toward its neighboring SLM molecule, forming pairs of interacting molecules. A magnetic field of ~ 3 G applied along $\hat{x}$ defines the quantization axis. Each pair of molecules interacts with a dipolar coupling

strength of

$$J = \frac{d^2}{4\pi\epsilon_0 r^3}(1 - 3\cos^2\alpha) \quad (1)$$

where d is the transition dipole moment for the $|\downarrow\rangle \leftrightarrow |\uparrow\rangle$ transition, $r = |\vec{r}|$ is the intermolecular separation, and α is the angle between $\vec{r}$ and the quantization axis. In most implementations, this coupling is tuned by changing r and, when angular control of α is needed, by reorienting the pair either in the transverse plane or by rotating the quantization field itself. In our apparatus, the three-dimensional degrees of freedom of an individual pair are specified through experimentally accessible parameters in cylindrical coordinates $(r_\perp, \theta, z_0)$, where $r_\perp$ is the magnitude of the projection of $\vec{r}$ onto the transverse $x-y$ plane, θ is its azimuthal angle relative to $\hat{x}$, and z_0 is the relative axial displacement (Fig. 1A, inset). The 2D-AODs provide rapid lateral positioning to set $(r_\perp, \theta)$, and the SLM hologram can independently impose z_0.

With the interaction geometry set, a Ramsey-$\pi/2$ microwave pulse is applied to prepare each pair of molecules in a superposition $(|\uparrow\rangle + |\downarrow\rangle)/\sqrt{2}$, which evolves under the dipolar Hamiltonian for a variable time. During this time we apply an XY8 dynamic decoupling sequence [8] to remove sources of single-body decoherence while preserving the dipolar interaction. A final Ramsey-$\pi/2$ pulse maps the dynamics onto two-qubit populations $(P_{\downarrow\downarrow}, P_{\uparrow\uparrow}, P_{\downarrow\uparrow}, P_{\uparrow\downarrow})$, corresponding to the probabilities of finding the pair in $(|\downarrow\downarrow\rangle, |\uparrow\uparrow\rangle, |\downarrow\uparrow\rangle, |\uparrow\downarrow\rangle)$, respectively.

Static geometric engineering of motional sensitivity

We begin by studying the motional sensitivity of the dipolar interaction and its dependence on geometry. Thermal motion of molecules broadens the distribution of the dipolar interaction J across the thermal ensemble by modifying both the intermolecular separation r and the angle θ. For CaF molecules in optical tweezers, the motional timescales set by the trap frequencies are orders of magnitude larger than the dipolar exchange dynamics. In this regime, the motional distribution is symmetric about the trap center and the linear sensitivity $\nabla J \cdot \delta\vec{r}$ averages to zero. The leading contribution to J is set by the width of the molecular wave packet, which is sampled from a thermal distribution [35]. Engineering the geometry of the interacting molecules is aimed at minimizing the quadratic sensitivity to the spatial extent of the molecular wave packet, while further cooling reduces the extent itself. Shifts of the mean trap positions, by contrast, enter through the linear term and are a first-order source of interaction dephasing.

In the simple planar configuration we first implement here - the two trap centers of an interacting molecule pair are constrained to the same focal plane ($z_0 = 0$) - the interaction geometry is set by a single in-plane angle θ, which can be tuned to the planar "magic" angle $\theta_m \approx 63.4°$, at which leading-order sensitivity of J to axial thermal motion vanishes, while the mean dipolar interaction remains nonzero [35]. This planar magic-angle condition, however, is only one slice of a more general three-dimensional geometry dependence and cannot additionally suppress dephasing arising from radial thermal motion. Introducing a finite axial displacement Δz between the two molecules adds an additional degree of freedom, allowing sensitivities of J to thermal motion along different spatial directions to be tuned simultaneously. To characterize this dependence, we define a dimensionless weighted relative sensitivity $\mathcal{S} \equiv \sum_i w_i |A_{i,2}|$, where $A_{i,2} \equiv (r^2/2J)\partial_i^2 J$ quantifies the leading-order (quadratic) change in J to displacement along direction i, and the normalized weights $w_i \propto 1/\omega_i^2$ account for trap anisotropy by weighting each axis by its relative thermal extent. In Fig. 1C we show $\mathcal{S}(\theta, z_0)$, where brighter regions correspond to geometries with reduced overall sensitivity of J to thermal motion.

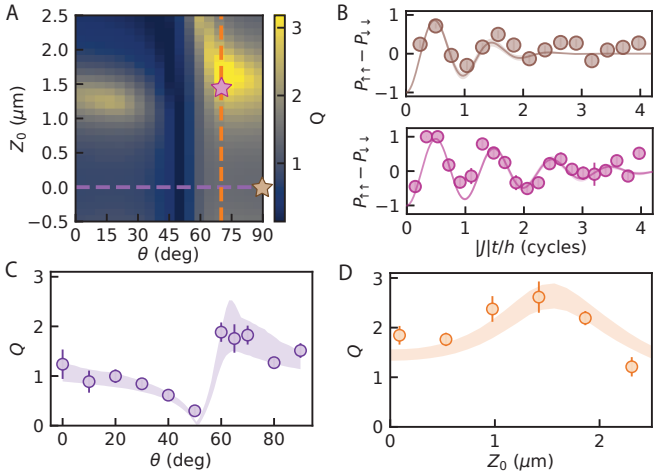

FIG. 2. **Static geometric engineering of dipolar interactions**. (**A**) Predicted interaction quality factor $Q = |J|\tau/h$ over geometry space parameterized by (θ, z_0). The stars mark the geometries used for the dipolar oscillation measurements shown in B, while the horizontal (vertical) dashed lines mark the cuts depicted in C (D). (**B**) Comparison of dipolar oscillations at a reference point $(\theta, z_0) = (90°, 0)$ and an optimal configuration $(\theta^*, z_0^*) = (70°, 1.42\,\mu\text{m})$. Solid lines are fit to a damped dipolar-exchange oscillation; corresponding fitted decay times are $\tau = 40(6)$ ms and 103(12) ms, respectively. (**C**) Dipolar interaction quality factor Q as a function of angle θ at $z_0 = 0$. (**D**) Dipolar quality factor Q as a function of z_0, at a fixed angle $\theta^* = 70°$. Shaded bands in (C, D) show the two-body dipolar model simulations, with widths indicating uncertainty from finite numerical sampling.

Guided by this geometric dependence, we next characterize the corresponding dipolar coherence across geometry space parametrized by (θ, z_0). We quantify this coherence by quality factor $Q \equiv |J|\tau/h$, where τ is the effective

$1/e$ decay time of the spin-exchange oscillation contrast, including finite single-body coherence. Fig. 2A shows the predicted Q for pairs of CaF molecules ($d \sim 1\,\mathrm{Debye}$) with an in-plane separation of $r_\perp = 2.5\ \mu$m. The two-body dipolar model is described in the supplementary material.

We first measure coherence in the planar configuration, with $z_0 = 0$. We vary the position of the AOD tweezers with respect to the static SLM tweezers, while maintaining a fixed magnetic field direction. The measured Q for a pair of molecules exhibits a slight optimum near $\theta^* \approx 63^\circ$ (Fig. 2C), consistent with the previously proposed 2D magic angle [35], despite the reduced interaction strength. The lack of a sharply peaked feature reflects the trade-off between enhanced coherence and reduced interaction strength J. The corresponding two-qubit population dynamics $P_{\uparrow\uparrow}$ and $P_{\downarrow\downarrow}$ measured at $(z_0 = 0, \theta^*)$, from which we extract the associated τ, is shown in Fig. 2B. The experimental measurements reported in this work are taken from a single representative molecule pair to avoid axial disorder in the SLM array [40] (Supplementary Text).

Having identified the optimal configuration within the planar geometry, we then vary the relative axial displacement z_0 at fixed θ^* by applying a variable offset of the defocus Zernike polynomial Z_2^0 on top of the base SLM phase hologram. Fig. 2D shows a peak in Q at finite offset $z_0^* \approx 1.42\,\mu$m. At this 3D "magic" configuration, we measure a maximum $Q = 2.61(31)$. The 3D magic configuration improves by approximately a factor of 1.4 relative to the 2D magic-angle case, demonstrating that the additional geometric degree of freedom can substantially enhance interaction coherence by reducing the motional sensitivity of J along all three axes. Representative dipolar spin-exchange dynamics measured at (θ^*, z_0^*) are shown in Fig. 2B.

Position noise and dynamic geometric echo

While the interleaved SLM-AOD array allows for precise and flexible control of the pairwise geometry, any differential fluctuation in their paths perturbs the mean trap positions of an interacting pair, resulting in a first-order change to the intermolecular spacing. These positional fluctuations are slow compared to the timescale of the dipolar interaction but can differ between experimental realizations, thereby introducing a dephasing channel in the coherent dipolar interactions. This positional disorder becomes increasingly consequential as we approach a magic configuration, since the sensitivity to thermal fluctuations is reduced. At these points, noise in relative position on the order of tens of nanometers can substantially limit the interaction coherence.

By imaging the two traps on a separate camera via a pick-off and feeding back on the tweezer position, we reduce the residual radial offset noise to approximately 50 nm rms over 24 hours (see Supplementary Text for measurement details). At magic configurations described above, with reduced thermal sensitivity, these fluctuations become the dominant source of dipolar decoherence. The ability to dynamically tune the geometry of the interacting molecules, on timescales faster than their entanglement rate, therefore opens a route to mitigating the effects of positional disorder.

We implement a two-step geometric echo that suppresses sensitivity to any static radial offsets. Since the relative position noise during the interaction is effectively static, it can be represented as a set of fixed offsets $(\Delta x, \Delta y, \Delta z)$. As illustrated in Fig. 3A, in the echo sequence, one molecule evolves for half of the sequence at position $(x + \Delta x, y + \Delta y, z + \Delta z)$ relative to the other molecule, and is then rapidly moved by the AODs to a symmetric geometry around $\hat{z}$ at $(-x + \Delta x, -y + \Delta y, z + \Delta z)$ for the second half of the interaction. In this way, the same positional disorder shifts the interaction strength in the opposite direction during the two equal segments, so any disorder-induced phase shifts cancel to first order while the desired interaction is preserved. In Fig. 3B, we compare dipolar oscillations taken at the separately optimized geometries with and without the echo protocol. Applying the echo protocol during dipolar interaction at the optimized 3D geometry ($\theta^* = 70^\circ, z_0^* = 1.8\ \mu$m) yields a dipolar coherence with $Q = 6.03(97)$ (Fig. 3B).

We quantify the robustness of this geometric echo protocol by injecting random radial offsets to the SLM trap positions and comparing the interaction Q factor with and without the geometric echo. We apply a different random grating on top of the SLM pattern every 10 seconds (see supplementary text). Fig. 3C shows the measured Q as a function of the magnitude of the injected disorder. At any scale of disorder the echo performs dramatically better than without the echo. At sufficiently large displacements the echo protocol does not cancel out higher-order effects, such as angle changes, and we see a degradation of the enhancement. This could be mitigated by using more complicated positional sequences [35]. In our present implementation, the geometric echo only targets transverse positional disorder. We estimate the uncanceled relative motion along the axial direction to be at the $\sim 50\,$nm level and attribute it mainly to thermally induced drift in the differential beam path.

Bell state characterization

Thus far, we have focused on using static and dynamic control over interaction geometry to suppress position fluctuations and reduce sensitivity to thermal motion. These techniques mitigate the first- and second-order sensitivities of the dipolar interaction to positional fluctuations. However, further cooling can still improve

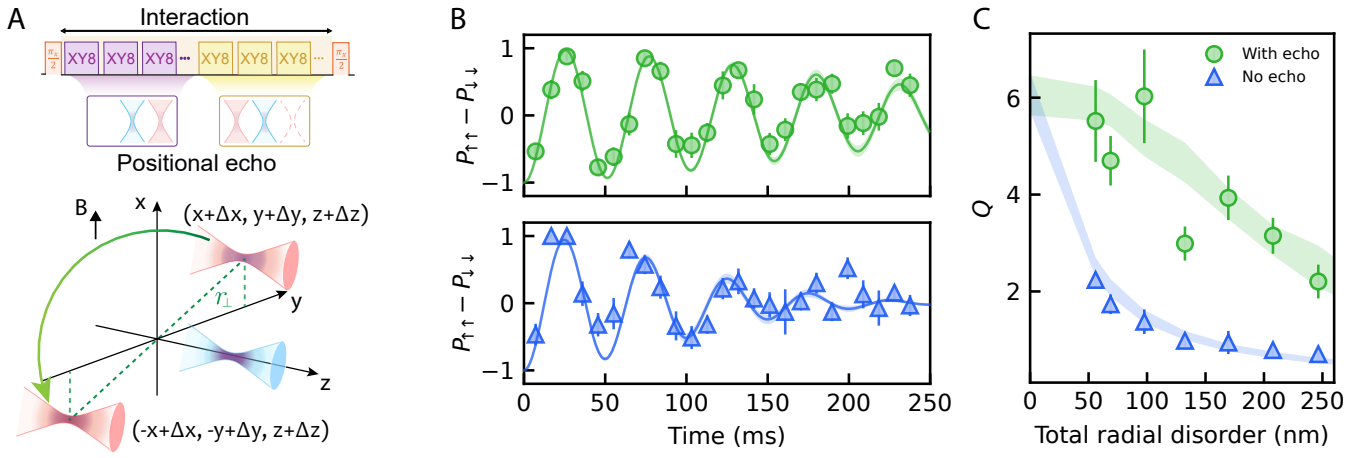

FIG. 3. **Positional Echo Protocol.** (**A**) The interacting pair evolves for equal durations at two geometries, realized by rapidly moving one molecule midway through the interaction duration. The XY8 dynamical decoupling sequence is applied throughout the interaction. (**B**) Comparison of optimal dipolar oscillations with the motional echo (top, green) and without the motional echo (bottom, blue). (**C**) We characterize the performance of the echo protocol by injecting additional disorder into the SLM trap position. The total radial disorder is obtained by adding the injected disorder in quadrature with the uncorrected baseline radial disorder ($\simeq 50$ nm); the first data points correspond to zero injected disorder. The echo protocol improves the dipolar coherence by a factor of 3.

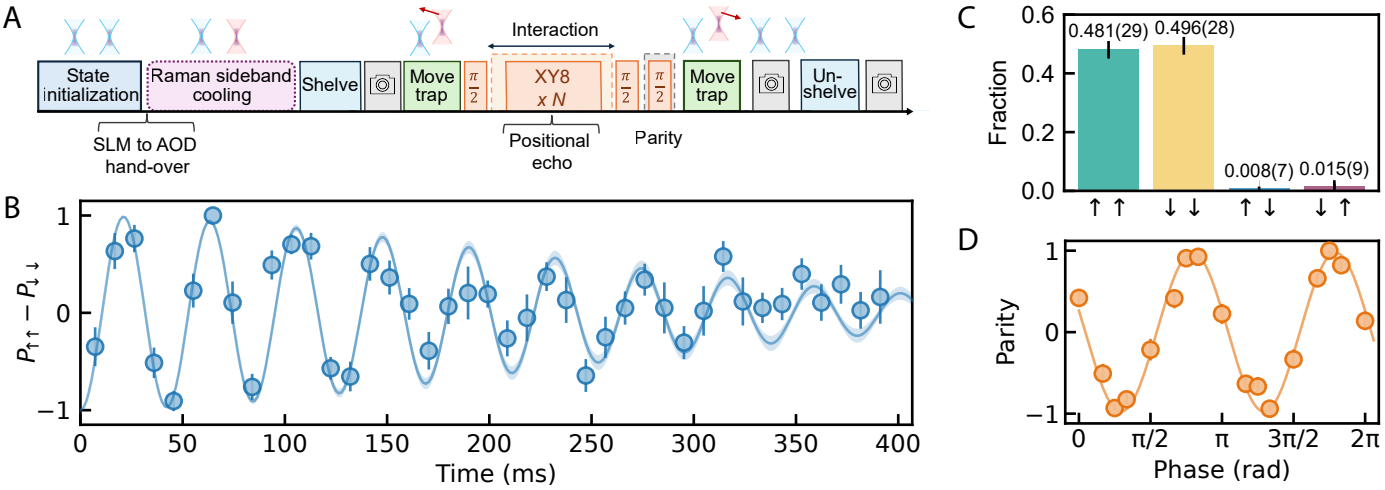

FIG. 4. **Optimal Configuration and Bell state characterization.** (**A**) Illustration of the experimental sequence. Molecules in the SLM and AOD traps are simultaneously Raman-sideband cooled and then moved to the interaction geometry. After the interaction, a $\pi/2$ analysis pulse with variable phase ϕ is used for parity measurement, followed by detection of both the $|\downarrow\rangle$ and $|\uparrow\rangle$ states. (**B**) A representative oscillation with $Q = 7.23(81)$. (**C**) Pair population statistics, measured in the computational basis at $t = 11.2$ ms of dipolar exchange evolution, corresponding to the $\pi/2$ point of the two-particle population oscillation. (**D**) Parity oscillations for a two-particle Bell state measured at the same evolution time. The fitted parity amplitude is $A_\Pi = 0.974^{+0.013}_{-0.018}$. Combining this with the pair populations in (C), we infer a Bell state fidelity of $\mathcal{F} = 0.976^{+0.008}_{-0.011}$.

coherence by reducing any residual quadratic contribution, as well as higher-order perturbations [35] that are not fully suppressed by geometric control. We combine these protocols with a partial Raman sideband cooling sequence [41] and benchmark the fidelity of a generated Bell state.

The experimental sequence is summarized schematically in Fig. 4A. After initializing all the molecules in $|\uparrow\rangle$, we apply partial Raman sideband cooling with the molecules already arranged and transferred to the interleaved array, as SLM-to-AOD trap handover after cooling can introduce substantial heating, especially at large axial displacements. To narrow the motional distribution while minimizing loss into weakly coupled motional states, we apply only a partial sideband cooling sequence, after which we estimate an axial occupation number of $\overline{n}_z \sim 10$ (Supplementary Text). As the final step of the cooling sequence also prepares the molecules

in the $|\downarrow\rangle$ state, molecules are then directly moved to the target interaction geometry, where they evolve under dipolar exchange with the geometric echo applied. In Fig. 4B, we show the resulting dipolar spin-exchange dynamics of partially cooled molecules at ($\theta = 70°, z_0 = 1.42\ \mu\text{m}, r_\perp = 1.9\ \mu\text{m}$), yielding an interaction quality factor $Q = 7.23(81)$, a 17% improvement relative to without sideband cooling. Since the geometry is fundamentally insensitive to temperature, further cooling to the motional ground state is only expected to provide a modest gain in dipolar coherence. Remaining decoherence is dominated by uncorrected axial position noise, while additional cooling cycles incur additional population loss (see Supplementary Text).

Using these experimental parameters, we generate a maximally entangled two-molecule Bell state by evolving the system for 1/4 of the oscillation period [8]. The state is characterized by the measured two-qubit populations and by a parity measurement, shown in Fig. 4C and D. After applying a $\pi/2$ pulse with variable phase ϕ, we measure the parity $\Pi(\phi) = P_{\uparrow\uparrow} + P_{\downarrow\downarrow} - P_{\uparrow\downarrow} - P_{\downarrow\uparrow}$. A sinusoidal fit yields the parity oscillation amplitude $A_\Pi = 0.974^{+0.013}_{-0.018}$ (Fig. 4D). Combining this with the measured populations $P_{\uparrow\uparrow} + P_{\downarrow\downarrow}$ (Fig. 4C), we infer a fidelity of $\mathcal{F} = 0.976^{+0.008}_{-0.011}$, conditioned on molecules surviving through state preparation and partial sideband cooling. This fidelity is comparable to previous exemplary demonstrations of entanglement with assembled polar molecules near their motional ground state ($\overline{n}_z < 1$) [10, 11], despite the molecules here having an axial occupation of $\overline{n}_z \sim 10$. The primary further limitations to improving dipolar coherence are threefold. First, the single-body coherence time is limited, partially due to black-body excitation between different vibrational states. Second, our current echo protocol does not cancel axial position disorder, which we estimate to be on the order of $\sim 50\,\text{nm}$ over the timescale of this measurement. Dynamic tweezers in three dimensions [42, 43], a cryogenic environment [44, 45], and magic-wavelength trapping [4] provide clear avenues for improvement. Third, improved cooling to $\overline{n}_z < 1$ would further reduce higher-order thermal effects. Each of these improvements compounds, and all three of these in conjunction would result in Bell state fidelities of $\mathcal{F} \geq 0.999$. Additional technical improvements and extensions of geometric control are discussed in the Supplementary Text.

Outlook

We have demonstrated that high-fidelity two-qubit entanglement of molecules can be reached through geometric control of the dipole-dipole interaction itself. The methods demonstrated here can be readily extended to other molecular tweezer platforms. Static three-dimensional geometry engineering reduces the sensitivity of the interaction to thermally induced motional broadening, while dynamic positional control refocuses slow relative positional noise between traps. This establishes a general strategy for suppressing quasi-static positional interaction disorder. Mitigating such disorder becomes increasingly important in larger arrays, where per-site calibration can be laborious, and when cooling lowers thermal broadening below the level of residual trap-position noise.

We have shown that a molecule can be moved during an entangling interaction without erasing the coherent dipolar evolution. Controlled motion thereby becomes not just a tool for assembly and rearrangement, but a corrective resource during the interaction. This places molecular tweezer arrays within a broader family of quantum processors in which motion is a coherent control resource. In trapped ions and neutral atoms, for example, transport has enabled reconfigurable connectivity while simply preserving quantum information [46–48]. Looking to the future, when geometry can be programmed on timescales that are short compared with the entangling dynamics, spatial control can be used as part of Hamiltonian engineering [35]. This opens routes to robust two-qubit gates [36, 49], geometry-echo-protected many-body dynamics [50], and programmable molecular systems in which the network of effective couplings [51, 52] can be dynamically engineered during coherent evolution.

ACKNOWLEDGMENTS

We are grateful to Wolfgang Ketterle for valuable discussions and helpful comments on the manuscript. This material is based upon work supported by the U.S. Department of Energy, Office of Science, National Quantum Information Science Research Centers, Quantum Systems Accelerator. Additional support is acknowledged from Harvard-MIT Center for Ultracold Atoms (Grant No. PHY-2317134); the Air Force Office of Scientific Research (AFOSR) AOARD under award number FA2386-24-1-4070; and from MURI W911NF-19-1-0283. S.S.Y. acknowledges support from the NSF GRFP. A.P. and S.S.Y. acknowledge support from the Harvard Quantum Initiative. Y.C. acknowledges support from the Quantum Information Research Support Center, funded by South Korea's Ministry of Science and ICT (MSIT) through the NRF of Korea (No. 2021M3H3A1036573). E.C. acknowledges support from the NRF of Korea (No. RS-2022-NR119745, RS-2024-00431938, RS-2024-00439981, and RS-2023-NR068116).

[1] J. W. Park, Z. Z. Yan, H. Loh, S. A. Will, and M. W. Zwierlein, Second-scale nuclear spin coherence time of

ultracold 23na40k molecules, Science **357**, 372 (2017).
[2] S. Burchesky, L. Anderegg, Y. Bao, S. S. Yu, E. Chae, W. Ketterle, K.-K. Ni, and J. M. Doyle, Rotational coherence times of polar molecules in optical tweezers, Physical Review Letters **127**, 123202 (2021).
[3] A. J. Park, L. R. Picard, G. E. Patenotte, J. T. Zhang, T. Rosenband, and K.-K. Ni, Extended rotational coherence of polar molecules in an elliptically polarized trap, Physical Review Letters **131**, 183401 (2023).
[4] P. D. Gregory, L. M. Fernley, A. L. Tao, S. L. Bromley, J. Stepp, Z. Zhang, S. Kotochigova, K. R. Hazzard, and S. L. Cornish, Second-scale rotational coherence and dipolar interactions in a gas of ultracold polar molecules, Nature Physics **20**, 415 (2024).
[5] T. R. Hepworth, D. K. Ruttley, F. von Gierke, P. D. Gregory, A. Guttridge, and S. L. Cornish, Long-lived multilevel coherences and spin-1 dynamics encoded in the rotational states of ultracold molecules, Nature Communications **16**, 7131 (2025).
[6] R. Sawant, J. A. Blackmore, P. D. Gregory, J. Mur-Petit, D. Jaksch, J. Aldegunde, J. M. Hutson, M. Tarbutt, and S. L. Cornish, Ultracold polar molecules as qudits, New Journal of Physics **22**, 013027 (2020).
[7] B. Sundar, B. Gadway, and K. R. Hazzard, Synthetic dimensions in ultracold polar molecules, Scientific reports **8**, 3422 (2018).
[8] Y. Bao, S. S. Yu, L. Anderegg, E. Chae, W. Ketterle, K.-K. Ni, and J. M. Doyle, Dipolar spin-exchange and entanglement between molecules in an optical tweezer array, Science **382**, 1138 (2023).
[9] C. M. Holland, Y. Lu, and L. W. Cheuk, On-demand entanglement of molecules in a reconfigurable optical tweezer array, Science **382**, 1143 (2023).
[10] L. R. Picard, A. J. Park, G. E. Patenotte, S. Gebretsadkan, D. Wellnitz, A. M. Rey, and K.-K. Ni, Entanglement and iswap gate between molecular qubits, Nature **637**, 821 (2025).
[11] D. K. Ruttley, T. R. Hepworth, A. Guttridge, and S. L. Cornish, Long-lived entanglement of molecules in magic-wavelength optical tweezers, Nature **637**, 827 (2025).
[12] J.-R. Li, W. G. Tobias, K. Matsuda, C. Miller, G. Valtolina, L. De Marco, R. R. Wang, L. Lassablière, G. Quéméner, J. L. Bohn, *et al.*, Tuning of dipolar interactions and evaporative cooling in a three-dimensional molecular quantum gas, Nature Physics **17**, 1144 (2021).
[13] J.-R. Li, K. Matsuda, C. Miller, A. N. Carroll, W. G. Tobias, J. S. Higgins, and J. Ye, Tunable itinerant spin dynamics with polar molecules, Nature **614**, 70 (2023).
[14] C. Miller, A. N. Carroll, J. Lin, H. Hirzler, H. Gao, H. Zhou, M. D. Lukin, and J. Ye, Two-axis twisting using floquet-engineered xyz spin models with polar molecules, Nature **633**, 332 (2024).
[15] Y. Lu, C. M. Holland, C. L. Welsh, X.-Y. Chen, and L. W. Cheuk, Probing coherent many-body spin dynamics in a molecular tweezer array quantum simulator, arXiv preprint arXiv:2603.19090 (2026).
[16] A. Micheli, G. K. Brennen, and P. Zoller, A toolbox for lattice-spin models with polar molecules, Nature Physics **2**, 341 (2006).
[17] A. V. Gorshkov, S. R. Manmana, G. Chen, J. Ye, E. Demler, M. D. Lukin, and A. M. Rey, Tunable superfluidity and quantum magnetism with ultracold polar molecules, Physical review letters **107**, 115301 (2011).
[18] B. Yan, S. A. Moses, B. Gadway, J. P. Covey, K. R. Hazzard, A. M. Rey, D. S. Jin, and J. Ye, Observation of dipolar spin-exchange interactions with lattice-confined polar molecules, Nature **501**, 521 (2013).
[19] K. R. Hazzard, B. Gadway, M. Foss-Feig, B. Yan, S. A. Moses, J. P. Covey, N. Y. Yao, M. D. Lukin, J. Ye, D. S. Jin, *et al.*, Many-body dynamics of dipolar molecules in an optical lattice, Physical review letters **113**, 195302 (2014).
[20] B. Gadway and B. Yan, Strongly interacting ultracold polar molecules, Journal of Physics B: Atomic, Molecular and Optical Physics **49**, 152002 (2016).
[21] L. Christakis, J. S. Rosenberg, R. Raj, S. Chi, A. Morningstar, D. A. Huse, Z. Z. Yan, and W. S. Bakr, Probing site-resolved correlations in a spin system of ultracold molecules, Nature **614**, 64 (2023).
[22] A. N. Carroll, H. Hirzler, C. Miller, D. Wellnitz, S. R. Muleady, J. Lin, K. P. Zamarski, R. R. Wang, J. L. Bohn, A. M. Rey, *et al.*, Observation of generalized tj spin dynamics with tunable dipolar interactions, Science **388**, 381 (2025).
[23] T. Bilitewski, L. De Marco, J.-R. Li, K. Matsuda, W. G. Tobias, G. Valtolina, J. Ye, and A. M. Rey, Dynamical generation of spin squeezing in ultracold dipolar molecules, Physical Review Letters **126**, 113401 (2021).
[24] D. DeMille, Quantum computation with trapped polar molecules, Physical Review Letters **88**, 067901 (2002).
[25] S. Yelin, K. Kirby, and R. Côté, Schemes for robust quantum computation with polar molecules, Physical Review A **74**, 050301 (2006).
[26] M. Karra, K. Sharma, B. Friedrich, S. Kais, and D. Herschbach, Prospects for quantum computing with an array of ultracold polar paramagnetic molecules, The Journal of chemical physics **144**, 094301 (2016).
[27] K.-K. Ni, T. Rosenband, and D. D. Grimes, Dipolar exchange quantum logic gate with polar molecules, Chemical science **9**, 6830 (2018).
[28] S. L. Cornish, M. R. Tarbutt, and K. R. Hazzard, Quantum computation and quantum simulation with ultracold molecules, Nature Physics **20**, 730 (2024).
[29] I. Kozyryev, Z. Lasner, and J. M. Doyle, Enhanced sensitivity to ultralight bosonic dark matter in the spectra of the linear radical sroh, Physical Review A **103**, 043313 (2021).
[30] D. DeMille, N. R. Hutzler, A. M. Rey, and T. Zelevinsky, Quantum sensing and metrology for fundamental physics with molecules, Nature Physics **20**, 741 (2024).
[31] T. Chupp, P. Fierlinger, M. Ramsey-Musolf, and J. Singh, Electric dipole moments of atoms, molecules, nuclei, and particles, Reviews of Modern Physics **91**, 015001 (2019).
[32] W. B. Cairncross and J. Ye, Atoms and molecules in the search for time-reversal symmetry violation, Nature Reviews Physics **1**, 510 (2019).
[33] I. Kozyryev and N. R. Hutzler, Precision measurement of time-reversal symmetry violation with laser-cooled polyatomic molecules, Phys. Rev. Lett. **119**, 133002 (2017).
[34] N. R. Hutzler, Polyatomic molecules as quantum sensors for fundamental physics, Quantum Science and Technology **5**, 044011 (2020).
[35] J. You, J. M. Doyle, Z. Liu, S. S. Yu, and A. Periwal, Control of dipolar dynamics by geometrical programming, Phys. Rev. Lett. **135**, 253002 (2025).

[36] M. Bergonzoni, S. Jandura, and G. Pupillo, iswap gate with polar molecules: Robustness criteria for entangling operations, Physical Review A **112**, 032621 (2025).
[37] Y. Bao, S. S. Yu, L. Anderegg, S. Burchesky, D. Gonzalez-Acevedo, E. Chae, W. Ketterle, K.-K. Ni, and J. M. Doyle, Fast optical transport of ultracold molecules over long distances, New Journal of Physics **24**, 093028 (2022).
[38] S. S. Yu, J. You, Y. Bao, L. Anderegg, C. Hallas, G. K. Li, D. Lim, E. Chae, W. Ketterle, K.-K. Ni, *et al.*, A conveyor-belt magneto-optical trap of caf, arXiv preprint arXiv:2409.15262 (2024).
[39] M. Endres, H. Bernien, A. Keesling, H. Levine, E. R. Anschuetz, A. Krajenbrink, C. Senko, V. Vuletic, M. Greiner, and M. D. Lukin, Atom-by-atom assembly of defect-free one-dimensional cold atom arrays, Science **354**, 1024 (2016).
[40] Y. T. Chew, M. Poitrinal, T. Tomita, S. Kitade, J. Mauricio, K. Ohmori, and S. de Léséleuc, Ultraprecise holographic optical tweezer array, Physical Review A **110**, 053518 (2024).
[41] Y. Bao, S. S. Yu, J. You, L. Anderegg, E. Chae, W. Ketterle, K.-K. Ni, and J. M. Doyle, Raman sideband cooling of molecules in an optical tweezer array to the 3d motional ground state, Physical Review X **14**, 031002 (2024).
[42] Y.-H. Lu, N. Song, T. Xiang, J. Ho, T.-C. Lee, Z. Yan, and D. M. Stamper-Kurn, Astigmatism-free 3d optical tweezer control for rapid atom rearrangement, arXiv preprint arXiv:2510.11451 (2025).
[43] L. R. Picard and M. Endres, A three-dimensional acousto-optic deflector, arXiv preprint arXiv:2510.07633 (2025).
[44] K.-N. Schymik, S. Pancaldi, F. Nogrette, D. Barredo, J. Paris, A. Browaeys, and T. Lahaye, Single atoms with 6000-second trapping lifetimes in optical-tweezer arrays at cryogenic temperatures, Physical Review Applied **16**, 034013 (2021).
[45] Z. Zhang, T.-W. Hsu, T. Y. Tan, D. H. Slichter, A. M. Kaufman, M. Marinelli, and C. A. Regal, High optical access cryogenic system for rydberg atom arrays with a 3000-second trap lifetime, PRX Quantum **6**, 020337 (2025).
[46] D. Bluvstein, H. Levine, G. Semeghini, T. T. Wang, S. Ebadi, M. Kalinowski, A. Keesling, N. Maskara, H. Pichler, M. Greiner, *et al.*, A quantum processor based on coherent transport of entangled atom arrays, Nature **604**, 451 (2022).
[47] J. M. Pino, J. M. Dreiling, C. Figgatt, J. P. Gaebler, S. A. Moses, M. Allman, C. Baldwin, M. Foss-Feig, D. Hayes, K. Mayer, *et al.*, Demonstration of the trapped-ion quantum ccd computer architecture, Nature **592**, 209 (2021).
[48] S. A. Moses, C. H. Baldwin, M. S. Allman, R. Ancona, L. Ascarrunz, C. Barnes, J. Bartolotta, B. Bjork, P. Blanchard, M. Bohn, *et al.*, A race-track trapped-ion quantum processor, Physical Review X **13**, 041052 (2023).
[49] A. E. Webb, S. C. Webster, S. Collingbourne, D. Bretaud, A. M. Lawrence, S. Weidt, F. Mintert, and W. K. Hensinger, Resilient entangling gates for trapped ions, Physical review letters **121**, 180501 (2018).
[50] J. Choi, H. Zhou, H. S. Knowles, R. Landig, S. Choi, and M. D. Lukin, Robust dynamic hamiltonian engineering of many-body spin systems, Physical Review X **10**, 031002 (2020).
[51] T. Bilitewski and A. M. Rey, Manipulating growth and propagation of correlations in dipolar multilayers: From pair production to bosonic kitaev models, Physical Review Letters **131**, 053001 (2023).
[52] O. Katz, L. Feng, D. Porras, and C. Monroe, Floquet control of interactions and edge states in a programmable quantum simulator, Nature Communications **16**, 8815 (2025).